Please refer to the following:
Jármai K. Farkas J; Snyman J A
Global minimum cost design of a welded square stiffened plate supported at four corners
STRUCTURAL AND MULTIDISCIPLINARY OPTIMIZATION (ISSN: 1615-147X) (eISSN: 1615-1488) 40: (1-6) pp. 477-489. (2010)

Global minimum cost design of a welded square stiffened plate supported at four corners*

József Farkas[1], Károly Jármai[2] and Jan A. Snyman[3]

[1,2]University of Miskolc, H-3515 Miskolc Hungary
[3]University of Pretoria, Pretoria 0002, South Africa
[1] altfar@uni-miskolc.hu**,** corresponding author
[2] altjar@uni-miskolc.hu, [3]jan.snyman@up.ac.za
* partially presented on the WCSMO7 congress in Seoul, South Korea

Abstract
This paper presents the application of a refined version of the original Snyman-Fatti (SF) global continuous optimization algorithm (Snyman, Fatti 1987) to the optimal design of welded square stiffened plates. In particular we investigate square plates of square symmetry subjected to uniformly distributed normal static loads, supported at four corners, and stiffened by a square symmetrical orthogonal grid of ribs. Halved rolled I-section stiffeners are used welded to the base plate by double fillet welds. Profiles of different size are used for internal and edge stiffeners.
A cost calculation method, developed by the first two authors and mainly used for welded structures (Farkas, Jármai 2003), allows for the computation of cost for different proposed designs of the welded stiffened plates. The cost function includes material, welding as well as painting costs, and is formulated according to the fabrication sequence. Design variables include base plate thickness as well as the dimensions of the edge and internal stiffeners. Constraints on stress in the base plate and in stiffeners, as well as on deflection of edge stiffeners and of internal stiffeners are considered. For this purpose the global unconstrained trajectory method of Snyman-Fatti is adapted to handle constraints of this type. For control purposes a particle swarm optimization algorithm is also applied to confirm the results given by the SF algorithm.
Since the torsional stiffness of open section stiffeners is very small, the stiffened plates are modelled as a torsionless gridwork. We present an algorithm for calculating the moments and deflections for torsionless gridworks with different number of internal stiffeners, using the force method.

Keywords: Structural optimization, Welded structures, Stiffened plates, Fabrication cost, Minimum cost design, Mathematical global optimization methods

1. Introduction

Stiffened plates are often used in various steel structures, e.g. in building roofs and floors, bridges, ships, offshore platforms etc. Structural characteristics of stiffened plates are as follows: material, loads, geometry of stiffening, supports, stiffener profile, number of stiffeners, fabrication technology and costs. A cost calculation method (Farkas, Jármai 1997) enables a realistic minimum cost design of welded stiffened plates and has been applied for various structural problems. One of these problems is the economy of stiffened plates and circular cylindrical shells. The costs of stiffened and unstiffened structural versions have been compared to each other to give conclusions for designers (Farkas et al. 2002, Farkas, Jármai 2005ab, Farkas 2005, Jármai et al. 2006).
In the present study a square plate is investigated subject to uniformly distributed normal static load, supported at four corners, stiffened by a square symmetrical orthogonal grid of ribs. Halved rolled I-section stiffeners are used and are welded to the base plate by double fillet welds (Fig.1).

The bending moments are calculated using the force method for torsionless gridworks with different numbers of stiffeners. Constraints on stress in the base plate and in stiffeners as well as on deflection of

edge stiffeners and of internal stiffeners are formulated. The cost function includes material, welding as well as painting costs and is formulated according to the fabrication sequence.
The design variables are the base plate thickness, the dimensions of edge and internal stiffeners and the number of internal stiffeners.
Fig.1 shows a schematic drawing of a square stiffened plate supported at four corners. In our study halved rolled I-section stiffeners are used with different dimensions for the edge stiffeners and for the internal stiffeners.

2. Geometric characteristics of stiffeners

In the calculation the notation is the same for internal and edge stiffeners. For edge stiffeners an additional *e* subscript is used.

Edge stiffeners are visible on Fig. 1.
Effective cross-sectional area

$$A_e = \frac{h_{1e}t_{we}}{2} + b_e t_{fe} + s_E t; s_E = 1.9t\sqrt{\frac{E}{f_y}} \tag{1}$$

where E is the Young modulus, f_y is the yield stress. The effective plate width s_E is calculated according to design rules of ECCS (1988).

$$h_{1e} = h_e - 2t_{fe} \tag{2}$$

The distances of the gravity centre G_e

$$z_{Ge} = \frac{1}{A_e}\left[\frac{h_{1e}t_{we}}{2}\left(\frac{h_{1e}}{4}+\frac{t}{2}\right) + b_e t_{fe}\left(\frac{h_e + t - t_{fe}}{2}\right)\right], \tag{3}$$

Figure 1. A schematic illustration of a stiffened square plate supported at four corners as well as the cross-sections of the edge and the internal stiffeners

$$z_{Ge1} = \frac{h_{1e} + t + 2t_{fe}}{2} - z_{Ge} \tag{4}$$

The moment of inertia

$$I_{ye} = s_E t z_{Ge}^2 + \frac{h_{1e}^3 t_{we}}{96} + \frac{h_{1e}t_{we}}{2}\left(\frac{h_{1e}}{4}+\frac{t}{2}-z_{Ge}\right)^2 + b_e t_{fe}\left(\frac{h_e + t - t_{fe}}{2} - z_{Ge}\right)^2 \tag{5}$$

We have neglected the flange plate inertia around their own centre of gravity. We have also neglected the fillets effect on the inertia. For internal stiffeners the same formulae hold but without index e (Fig. 1).

3. Costs as a function of number of internal stiffeners (*n*) in one direction

The corresponding structural volumes are as follows.

$$V_0 = L^2 t;\ V_1 = V_0 + 4A_{eS}L;\ V_2 = V_1 + nLA_S; \tag{6}$$

$$V_3 = V_2 + nLA_S;\ A_{eS} = b_e t_{fe} + h_{1e}t_{we}/2\ ; \tag{7}$$

$$A_S = bt_f + h_1 t_w/2 \tag{8}$$

where L is the length of the square plate (L = 18 m in the example).
Welding of the base plate with 36 plate parts of dimension 6x1.5 m using GMAW-C (gas metal arc welding with CO_2 gas) single-bevel welds with complete joint penetration

$$K_{F1} = k_F\left(\Theta\sqrt{36\rho V_0} + 1.3C_W x10^{-3} t^{n1} 13L\right) \tag{9}$$

where k_F is the specific fabrication cost, ρ is the material density, C_w is the welding technology parameter, Θ is the difficulty parameter. In the multiplier 1.3 the additional welding times are considered.
The welding cost function contains two parts: the first part of the equation means the preparation time, where the number and volume of the elements are important, second part contains the real welding time and some additional process times.
Welding of four edge stiffeners to the base plate (5 elements in total) by double fillet welds using GMAW-C

$$K_{F2} = k_F\left(\Theta\sqrt{5\rho V_1} + 1.3x0.3394x10^{-3}a_{we}^2 8L\right) \quad (10)$$

where the welding joint size is a_{we}, $0.3394x10^{-3}$ is the welding technology parameter. Edge stiffeners are welded together at the corners, but this welding time is neglected.

$a_{we} = 0.4t_{we}$, but $a_{we.min} = 3$ mm (11)

Welding of n continuous internal stiffeners to the base plate and to the edge stiffeners by double fillet welds using GMAW-C

$$K_{F3} = k_F\left[\Theta\sqrt{(n+1)\rho V_2} + 1.3x0.3394x10^{-3}a_w^2 2n(L + h_1 + 2b)\right] \quad (12)$$

where the welding joint size is a_w

$a_w = 0.4t_w$, but $a_{w.min} = 3$ mm (13)

Welding of n intermittent internal stiffeners to the base plate, to the edge stiffeners and to the continuous internal stiffeners (at the internal nodes butt welds are used for connection of bottom flanges)

$$K_{F4} = k_F\left\langle\Theta\sqrt{[(n+1)n+1]\rho V_3} + 1.3x0.3394x10^{-3}a_w^2\{2nL + 2(n+1)nh_1 + 2n(n+4)b\} + T_1\right\rangle$$

$$T_1 = 1.3C_w t_f^{n1} 2n^2 b \quad (14)$$

for butt welds using GMAW-C

for t_f<15 mm C_w =0.1939x10^{-3}, $n_1 = 2$ (15a)

for t_f >15 mm C_w = 0.1496x10^{-3}, n_1 = 1.9029 (15b)

Cost of material is proportional to the volume, density and the specific fabrication cost parameter

$$K_M = k_M \rho V_3 \quad (16)$$

where k_M is the specific material cost.

Cost of painting is proportional to the painted surface area (S_P), the difficulty factor (Θ_P) and the specific painting cost parameter (k_P)

$$K_P = \Theta_P k_P S_P \quad (17)$$

$$S_P = 2L^2 + 4L(h_{1e} + 2b_e) + 2n^2 L(h_1 + 2b) \quad (18)$$

Total cost is the sum of the previous cost elements

$K = K_M + K_{F1} + K_{F2} + K_{F3} + K_{F4} + K_P$ (19)

4. Constraints

Stresses in edge stiffeners from bending moment M_e in the top fiber and from local bending of the base plate

$$\sigma_e = \frac{M_e}{I_{ye}} z_{Ge} + cp_0 \frac{a^2}{t^2} \le f_{y1} \quad (20)$$

where the distance between the internal stiffeners is $a = \frac{L}{n+1}$, p_0 is the factored uniformly distributed load.

c = 0.3078, the value comes form Timoshenko & Woinowsky-Krieger, S. (1959) page 202, in which the maximum bending moment in the square plate with all edges built in is $M = 0.0513\ pa^2$ and the section modulus of the plate is $t^2/6$. The stress of the base plate is always larger at the edges than in the middle see Timoshenko & Woinowsky-Krieger, S. (1959), so there is no constraint defined for the base plate.

In the calculation of the first term of Eq. (20) the stress in the center line of the base plate is considered.

Stress in edge stiffener bottom fiber from the bending moment

$$\sigma_{e1} = \frac{M_e}{I_{ye}} z_{Ge1} \le f_{y1} \quad (21)$$

Stresses in the internal stiffeners from bending moment M in the top fiber and from local bending of the base plate

$$\sigma = \frac{M}{I_y} z_G + cp_0 \frac{a^2}{t^2} \le f_{y1} \quad (22)$$

In the calculation of the first term of Eq. (22) the stress in the center line of the base plate is considered.

Stress in the internal stiffener bottom fiber from bending moment

$$\sigma_1 = \frac{M}{I_y} z_{G1} \le f_{y1} \tag{23}$$

Deflection of the edge stiffeners

$$w_e \le w_{adm} \tag{24}$$

Deflection of the internal stiffener

$$w_1 \le w_{adm} \tag{25}$$

Bending moments and deflections should be derived for each number of internal stiffeners n.

Stability considerations

The constraint on the local buckling of the based plate is considered by calculation of the effective plate width. The rolled stiffeners have no stability problems.

5. Numerical data

Yield stress of steel f_y = 355 MPa, $f_{y1} = f_y/1.1$, elastic modulus $E = 2.1\text{x}10^5$ MPa, edge length of the base plate L = 18.0 m, factored load intensity p_0 = 0.0015 N/mm^2, load intensity considering the self mass

$$p = p_0 + \rho_0 \frac{V_3}{L^2}, \tag{26}$$

density of steel $\rho = 7.85x10^{-6}$ kg/mm^3, $\rho_0 = 7.85x10^{-5}$ N/mm^3,

admissible deflection $w_{adm} = L/300$,

factor for the complexity of assembly $\Theta = 3$, factor for the complexity of painting $\Theta_P = 3$,

cost factors: k_M = 1.0 \$/kg, k_F = 1.0 \$/min, $k_P = 14.4\text{x}10^{-6}$ \$/mm^2.

The ranges of unknowns: t = 4 – 40 mm, h and h_e = 152 – 1008.1 mm.

The discrete values of h and the nominal size of I-beam (UB)(in the parenthesis) are as follows according to ARCELOR catalogue: 152.4 (152), 177.8 (178), 203.2 (203), 257.2 (254), 308.7 (305), 353.4 (356), 403.2 (406), 454.6 (457), 533.1 (533), 607.6 (610), 683.5 (686), 762.2 (762), 840.7 (838), 910.4 (914), 1008.1 (1016) mm.

Approximate expressions for other dimensions of rolled I-profiles as a function of h or h_e according to the ARCELOR catalogue are detailed in Appendix.

6. Special case of three internal stiffeners (n = 3) (Fig.2)

The internal forces in the nodes of the gridwork are F_1, F_2 and F_3 (Fig.2), since in the nodes locating in the diagonals internal forces do not occur because of square symmetry. The unknown forces can be determined by solving two equilibrium, and one deflection equation.

The equilibrium equations are as follows (Fig.2):

$$2pa^2 + F_1 = 2F_3 \tag{27}$$

$$2pa^2 - 2F_1 = 2F_2 \tag{28}$$

The deflection equation expresses the fact that the two internal stiffeners in the nodes No.1 have the same deflection

$$w_{13} - w_{30} = w_{12} - w_{20} \tag{29}$$

where w_{30} and w_{20} are the deflections of the edge stiffeners.

$$EI_{ye} w_{20} = \frac{5pL^5}{48x8x16} + \frac{F_2 L^3}{48} + \frac{11F_3 L^3}{6x64} \tag{30}$$

$$EI_{ye} w_{30} = \frac{57pL^5}{48x32x64} + \frac{11F_2 L^3}{12x64} + \frac{F_3 L^3}{48} \tag{31}$$

Figure 2. Square plate with three internal stiffeners in one direction. Internal forces and deflections

$$EI_y w_{13} = \frac{5pL^5}{48x64} + \frac{F_1 L^3}{48} \tag{32}$$

$$EI_y w_{12} = \frac{57pL^5}{48x64x16} - \frac{F_1 L^3}{48} \tag{33}$$

Introducing the notation $\eta = I_{ye} / I_y$ one obtains the equation

$$\frac{11.5pL^2}{64} + \frac{23pL^2\eta}{64} + 32F_1\eta + 5F_2 + 6F_3 = 0 \tag{34}$$

Together with the equilibrium equations the solution of the three equations is

$$F_1 = -\frac{pL^2}{256(16\eta - 1)}(46\eta + 111) \tag{35}$$

$$F_2 = \frac{pL^2}{16} - F_1 \tag{36}$$

$$F_3 = \frac{pL^2}{16} + \frac{F_1}{2} \tag{37}$$

The maximum bending moment in the edge stiffeners

$$M_e = \frac{pL^3}{16x8} + \frac{F_A L}{2} - \frac{F_3 L}{4}, F_A = \frac{pL^2}{16} + \frac{F_2}{2} + F_3 \tag{38}$$

and in the internal stiffener

$$M = \frac{pL^3}{16x4} + \frac{F_1 L}{4} \tag{39}$$

The constraint on maximum deflection for an edge stiffener is expressed as

$$w_e = w_{20.0} \le L/300 \tag{40}$$

and for an internal stiffener

$$w_1 = w_{13.0} \le L/300 \tag{41}$$

$w_{20.0}$ and $w_{13.0}$ should be calculated with p_0 instead of p, it means that the self weight is neglected:

$$F_{10} = -\frac{p_0 L^2}{256(16\eta - 1)}(103\eta + 111) \tag{42}$$

$$F_{20} = \frac{p_0 L^2}{16} - F_{10} \tag{43}$$

$$F_{30} = \frac{p_0 L^2}{16} + \frac{F_{10}}{2} \tag{44}$$

$$w_{20.0} = \frac{5p_0 L^5}{48x8x16EI_{ye}} + \frac{F_{20}L^3}{48EI_{ye}} + \frac{11F_{30}L^3}{6x64EI_{ye}} \tag{45}$$

$$w_{13.0} = \frac{5p_0 L^5}{48x64EI_y} + \frac{F_{10}L^3}{48EI_y} \tag{46}$$

7. Special case of four internal stiffeners (n = 4) (Fig.3)

Similar than in the case of n = 3, there are also three unknown forces F_2, F_3 and F_5, since in the nodes No.1 and No.4 internal forces do not occur because of symmetry. The calculation is similar, but to demonstrate the difficulty of determination of grid forces and moments, it is described in details. The two equilibrium equations are as follows:

$$\frac{5}{2}pa^2 + 2F_2 = 2F_5 \tag{47}$$

$$\frac{5}{2}pa^2 - 2F_2 = 2F_3 \tag{48}$$

The deflection equation is expressed as

$$w_{23} - w_{30} = w_{25} - w_{50} \tag{49}$$

where

$$EI_y w_{23} = \frac{29pa^5}{12} - \frac{11F_2a^3}{6} \tag{50}$$

$$EI_y w_{25} = \frac{31pa^5}{8} + \frac{14F_2a^3}{3} \tag{51}$$

$$EI_{ye} w_{30} = \frac{31pa^5}{16} + \frac{14F_3a^3}{3} + \frac{17F_5a^3}{6} \tag{52}$$

$$EI_{ye} w_{50} = \frac{29pa^5}{24} + \frac{17F_3a^3}{6} + \frac{11F_5a^3}{6} \tag{53}$$

Solving the two equilibrium and one deflection equation one obtains

$$F_3 = \frac{460\eta + 155}{312\eta - 40} pa^2 \tag{54}$$

Figure 3. Square plate with four internal stiffeners in one direction. Internal forces and deflections

$$F_2 = \frac{F_5}{2} - \frac{F_3}{2} \tag{55}$$

$$F_5 = \frac{5pa^2}{2} - F_3 \tag{56}$$

The maximum bending moment in the edge stiffener is given by

$$M_e = \frac{pL^3}{160} + \frac{2F_3L}{5} + \frac{F_5L}{5} \tag{57}$$

The maximum bending moment in the internal stiffeners is the larger of the following two values

$$M_3 = \frac{pL^3}{80} - \frac{F_2L}{5} \tag{58}$$

$$M_5 = \frac{pL^3}{80} + \frac{2F_2L}{5} \tag{59}$$

$$M = max(M_3, M_5) \tag{60}$$

Deflection constraints should be calculated with forces using p_0 instead of p:

$$F_{30} = \frac{460\eta + 155}{312\eta - 40} p_0a^2, F_{50} = \frac{5p_0a^2}{2} - F_{30} \tag{61}$$

Deflection constraint for edge stiffeners

$$w_e = \frac{1}{EI_{ye}} \left(\frac{3125p_0a^5}{384x4} + \frac{59F_{30}a^3}{12} + \frac{71F_{50}a^3}{24} \right) \le \frac{L}{300} \tag{62}$$

and for internal stiffener

$$w_1 = \frac{1}{EI_y} \left(\frac{3125p_0a^5}{384x2} + \frac{59F_2a^3}{12} \right) \le \frac{L}{300} \tag{63}$$

8. Special case of five internal stiffeners (n = 5) (Fig.4)

Unknowns: F_2, F_4, F_5, F_6, F_8, F_9

Equilibrium equations:

$3pa^2 + 2F_5 + F_4 = 2F_9$ (64)

$3pa^2 - 2F_5 + F_2 = 2F_8$ (65)

$3pa^2 - 2F_4 - 2F_2 = 2F_6$ (66)

Figure 4. Square plate with five internal stiffeners in one direction. Internal forces and deflections

Deflection equations:
For the node 5

$$w_{59} - w_{90} = w_{58} - w_{80} \tag{67}$$

For the node 4

$$w_{49} - w_{90} = w_{46} - w_{60} \tag{68}$$

For the node 2

$$w_{28} - w_{80} = w_{26} - w_{60} \tag{69}$$

The deflections are as follows
for edge stiffener

$$EI_{ye} w_{60} = \frac{135pa^5}{32} + \frac{9F_6a^3}{2} + \frac{23F_8a^3}{3} + \frac{13F_9a^3}{3} \tag{70}$$

$$EI_{ye} w_{80} = \frac{11pa^5}{3} + \frac{23F_6a^3}{6} + \frac{20F_8a^3}{3} + \frac{23F_9a^3}{6} \tag{71}$$

$$EI_{ye} w_{90} = \frac{205pa^5}{96} + \frac{13F_6a^3}{6} + \frac{23F_8a^3}{6} + \frac{7F_9a^3}{3} \tag{72}$$

for the stiffener 9-9

$$EI_y w_{59} = \frac{22pa^5}{3} + \frac{23F_4a^3}{6} + \frac{20F_5a^3}{3} \tag{73}$$

$$EI_y w_{49} = \frac{135pa^5}{16} + \frac{9F_4a^3}{2} + \frac{23F_5a^3}{3} \tag{74}$$

for the stiffener 8-8

$$EI_y w_{58} = \frac{205pa^5}{48} + \frac{13F_2a^3}{6} - \frac{7F_5a^3}{3} \tag{75}$$

$$EI_y w_{28} = \frac{135pa^5}{16} + \frac{9F_2a^3}{2} - \frac{13F_5a^3}{3} \tag{76}$$

for the stiffener 6-6

$$EI_y w_{46} = \frac{205pa^5}{48} - \frac{23F_2a^3}{6} - \frac{7F_4a^3}{3} \tag{77}$$

$$EI_y w_{26} = \frac{22pa^5}{3} - \frac{20F_2a^3}{3} - \frac{23F_4a^3}{6} \tag{78}$$

After the substitution of Eqs (70-78) into Eqs (67, 68 and 69) one obtains

$$-208F_2\eta + 368F_4\eta + 864F_5\eta + 160F_6 + 272F_8 + 144F_9 = -147pa^2(1+2\eta) \tag{79}$$

$$368F_2\eta + 656F_4\eta + 736F_5\eta + 224F_6 + 368F_8 + 192F_9 = -200pa^2(1+2\eta) \tag{80}$$

$$1072F_2\eta + 368F_4\eta - 416F_5\eta + 64F_6 + 96F_8 + 48F_9 = -53pa^2(1+2\eta) \tag{81}$$

After the solution of six equations (64, 65, 66, 79, 80, 81) we calculate the bending moments and deflections to check the constraints. The maximum bending moment in the edge stiffener can be expressed as

$$M_e = \frac{9pa^3}{8} + 3F_A a - 2F_9 a - F_8 a \tag{82}$$

The governing bending moment in the internal stiffeners M is the maximum from the following three bending moments

$$M_1 = \frac{9pa^3}{4} + 3F_9 a - F_5 a \tag{83}$$

$$M_2 = \frac{9pa^3}{4} + 3F_8 a + 2F_5 a \tag{84}$$

$$M_3 = \frac{9pa^3}{4} + 3F_6a + 2F_4a + F_2a \tag{85}$$

$$M = max(M_1, M_2, M_3) \tag{86}$$

Deflection constraints should be calculated with forces using p_0 instead of p (F_{20},F_{40},F_{50},F_{60},F_{80},F_{90}):

$$w_e = w_{60} = \frac{1}{EI_{ye}}\left(\frac{135p_0a^5}{32} + \frac{9F_{60}a^3}{2} + \frac{23F_{80}a^3}{3} + \frac{13F_{90}a^3}{3}\right) \le \frac{L}{300} \tag{87}$$

$$w_1 = \frac{1}{EI_y}\left(\frac{135p_0a^5}{16} - \frac{23F_{20}a^3}{3} - \frac{13F_{40}a^3}{3}\right) \le \frac{L}{300} \tag{88}$$

9. Mathematical optimization methods

9.1. General formulation of design optimization problem

In the case of the welded square stiffened plate the design variables are t, h and h_e. The cost function K, also called the objective function, and the constraints clearly depend on these variables. Different number of internal stiffeners means a special case of the welded square stiffened plate design, with different internal forces and deflections. In more general optimization notation, the design vector is denoted by $\boldsymbol{x} = [x_1, x_2, x_3]^{\mathrm{T}} = [t, h, h_e]^{\mathrm{T}}$, and the objective function by $f(\boldsymbol{x})=K(\boldsymbol{x})$. The constraints, here (20, 21, 22, 23, 24, 25), may be written in the standard inequality form as $g_j(\boldsymbol{x}) \le 0, \quad j = 1,..6$. More explicitly the constraints are:

$$\begin{aligned}
&g_1(\boldsymbol{x}) = \sigma_e(\boldsymbol{x}) - f_{y1} \le 0\\
&g_2(\boldsymbol{x}) = \sigma_{e1}(\boldsymbol{x}) - f_{y1} \le 0\\
&g_3(\boldsymbol{x}) = \sigma(\boldsymbol{x}) - f_{y1} \le 0\\
&g_4(\boldsymbol{x}) = \sigma_1(\boldsymbol{x}) - f_{y1} \le 0\\
&g_5(\boldsymbol{x}) = w_e(\boldsymbol{x}) - w_{adm} \le 0\\
&g_6(\boldsymbol{x}) = w_1(\boldsymbol{x}) - w_{adm} \le 0
\end{aligned} \tag{89}$$

Thus it is required to minimize, for each specified number of internal stiffeners (n=3,4,5), the objective function $f(\boldsymbol{x})=K(\boldsymbol{x})$ given by (19), subject to the inequality constraints (89).

Before presenting the optimization results we briefly summarize the basics of the optimization algorithms used here, namely the Snyman-Fatti (SF) global trajectory method and also the Particle Swarm Optimization (PSO) method that was used as a control.

9.2 The Snyman-Fatti method

The global method used here, namely the Snyman-Fatti (SF) multi-start global minimization algorithm with dynamic search trajectories for global continuous unconstrained optimization (Snyman, Fatti 1987, (Groemwold, Snyman 2002), was recently reassessed and refined (Snyman, Kok 2007) to improve its efficiency and to be applicable to constrained problems. The resultant improved computer code has been shown to be competitive with of the best evolutionary global optimization algorithms currently available when tested on standard test problems (Snyman 2005). Here we wish to apply it to the practical stiffened plate problem outlined in the previous sections. For a detailed presentation and discussion of the motivation and theorems on which the SF algorithm is based, the reader is referred to the original paper of Snyman and Fatti (1987). Here we restrict ourselves to a summary giving the essentials of the multi-start global optimization methodology using dynamic search trajectories.

Consider the general inequality constrained problem:

$$\underset{w.r.t.\ \boldsymbol{x}}{\text{minimize}} \quad f(\boldsymbol{x}),\ \boldsymbol{x} = [x_1, x_2, \mathrm{K}\ x_n]^T \in R^n, \tag{90}$$

subject to the inequality constraints:

$$g_j(\boldsymbol{x}) \le 0, \quad j = 1,2,\text{K},m$$

The optimum solution to this problem is denoted by $\boldsymbol{x}^*$ with associate optimum function value $f(\boldsymbol{x}^*)$.

We address the constrained problem (90) by transforming it to an unconstrained problem via the formulation of the penalty function $F(\boldsymbol{x})$, to which the unconstrained global SF optimization algorithm is applied. The penalty function $F(\boldsymbol{x})$ is defined as

$$F(\boldsymbol{x}) = f(\boldsymbol{x}) + \sum_{j=1}^{m} \rho_j \{ g(\boldsymbol{x}) \}^2 \tag{91}$$

where $\rho_j = 0$ if $g_j(\boldsymbol{x}) \le 0$, else $\rho_j = \mu$ (a large number). $g(\boldsymbol{x})^2$ is used to ensure that the second part is positive and to increase its value.

Thus we consider the unconstrained global optimization problem that can be stated: for a continuously differentiable objective function $F(\boldsymbol{x})$: find a point $\boldsymbol{x}^*(\mu)$ in the set $X \subset R^n$ such that
$F^* = F(\boldsymbol{x}^*(\mu)) =$ minimum of $F(\boldsymbol{x})$ over $\boldsymbol{x} \in X$ (92)

The SF algorithm applied to this problem, is basically a multi-start technique in which several starting points are sampled in the domain of interest X (usually defined by a box in R^n), and a local search procedure is applied to each sample point. The method is heuristic in essence with the lowest minimum found after a finite number of searches being taken as an estimate of F^*.

In the local search the SF algorithm explores the variable space X using search trajectories derived from the differential equation:

$$\ddot{\boldsymbol{x}} = -\nabla F(\boldsymbol{x}(t)) \tag{93}$$

where ∇F is the gradient vector of $F(\boldsymbol{x})$. Equation (93) describes the motion of a particle of unit mass in an n-dimensional conservative force field, where $F(\boldsymbol{x}(t))$ represents the potential energy of the particle at position $\boldsymbol{x}(t)$. The search trajectories generated here are similar to those used in Snyman's dynamic method for local minimization (Snyman 1982, 1983). In the SF global method, however, the trajectories are modified in a manner that ensures, in the case of multiple local minima, a higher probability of convergence to a lower local minimum than would have been achieved had conventional gradient local search methods been used. The specific modifications employed result in an increase in the *regions of convergence* of the lower minima including, in particular, that of the global minimum. A stopping rule, derived from a Bayesian probability argument, is used to decide when to end the global sampling and accept the current overall minimum value of F, taken over all sampling points to date, as the global minimum F^*.

For initial conditions, position $\boldsymbol{x}(0) = \boldsymbol{x}^0$ and velocity $\dot{\boldsymbol{x}}(0) = \boldsymbol{v}(0) = \boldsymbol{v}^0 = \boldsymbol{0}$, integrating (93) from time 0 to t, implies the energy conservation relationship:

$$\tfrac{1}{2}\|\boldsymbol{v}(t)\|^2 + F(\boldsymbol{x}(t)) = \tfrac{1}{2}\|\boldsymbol{v}(0)\|^2 + F(\boldsymbol{x}(0)) = F(\boldsymbol{x}(0)) \tag{94}$$

The first term on the left-hand side of (94) represents the kinetic energy, whereas the second term represents the potential energy of the particle of unit mass, at any instant t. Obviously the particle will start moving in the direction of steepest descent and its kinetic energy will increase, and thus F will decrease, as long as it moves downhill, i.e. as long as $-\nabla F \cdot \boldsymbol{v} > 0$, where $\cdot$ denotes the scalar product.

If descent is not met along the generated path then the magnitude of the velocity $\boldsymbol{v}$ decreases as it moves uphill and its direction changes towards a local minimizer. If the possibility of more than one local minimizer exists and we are interested in finding the global minimum, a realistic global strategy is to monitor the trajectory and record the point $\boldsymbol{x}^m$ and corresponding velocity $\boldsymbol{v}^m = \dot{\boldsymbol{x}}^m$ and function value F^m at which the minimum along the path occurs, letting the particle continue uninterrupted along its path with conserved energy. This is done in the hope that it may surmount a ridge of height F^r, $F^m < F^r < F(\boldsymbol{x}(0))$, continuing further along a path that may lead to an even lower value of F beyond the ridge. On the other hand it is necessary to terminate the trajectory before it retraces itself or approximately retraces itself in indefinite periodic or ergodic (space-filling) motion. A proper termination condition that employed in the SF algorithm, is to stop the first trajectory once it reaches a point with a function value close to its starting

value $F^s=F(\boldsymbol{x}(0))$ while still moving uphill, i.e. while $\nabla F\cdot\boldsymbol{v}>0$. At this point, once termination has occurred and after setting the best point $\boldsymbol{x}^b:=\boldsymbol{x}^m$ with corresponding function value $F^b:=F^m$, it is proposed that a further auxiliary or inner trajectory be started from a new inner starting point $\boldsymbol{x}^s:=\frac{1}{2}(\boldsymbol{x}^0+\boldsymbol{x}^b)$ with initial velocity $\frac{1}{2}\boldsymbol{v}^m$ and associated starting function value $F^s=F(\boldsymbol{x}^s)$. Again for this new auxiliary or inner trajectory the function value is monitored, and for this new trajectory $\boldsymbol{x}^m$ and associated $\boldsymbol{v}^m$ are recorded anew. On its termination, again once the function value approaches F^s sufficiently closely while moving uphill, the starting point for the next inner trajectory is taken as $\boldsymbol{x}^s=\frac{1}{2}(\boldsymbol{x}^s+\boldsymbol{x}^b)$ with initial velocity $\frac{1}{2}\boldsymbol{v}^m$, where $\boldsymbol{x}^b$ again corresponds to the overall best point for the current sampling point. This generation of successive inner trajectories is continued until $\boldsymbol{x}^b$ converges or $\nabla F(\boldsymbol{x}^b)$ is effectively zero.

Of course, the above strategy assumes that the trajectory obtained from the solution of differential equation (93) is exactly known at all time instances. In practice this is not possible, and the generation of the trajectories is done numerically by means of the leap-frog scheme [14]: Given initial position $\boldsymbol{x}^0=\boldsymbol{x}(0)$ and initial velocity $\boldsymbol{v}^0=\boldsymbol{v}(0)=\dot{\boldsymbol{x}}(0)$ and a time step Δt, compute for k=0,1,2,…

$$\boldsymbol{x}^{k+1}=\boldsymbol{x}^k+\boldsymbol{v}^k\Delta t \qquad (95)$$
$$\boldsymbol{v}^{k+1}=\boldsymbol{v}^k-\nabla F(\boldsymbol{x}^{k+1})\,\Delta t$$

A heuristic procedure is used to select an appropriate time step Δt (Snyman, Kok 2007). Once the sequence of inner (auxiliary) trajectories for the current iteration (i.e. current random starting point) is terminated the local minimum $\boldsymbol{x}^{k+1}$ with function value F^{k+1} obtained at that iteration, is evaluated for its probability of being the global minimum. This global component of the algorithm involves a stochastic criterion that reports the probability of the lowest obtained minimum to be the global one (Snyman, Fatti 1987). To this end, let R_j denote the region of convergence of a local minimum $\hat{F}_j$ in the search space, and α_j denote the probability that a randomly selected point falls within R_j. Let R^* and α^* denote the corresponding quantities for the global minimum F^*. Snyman and Fatti (1987) then argue that, because of its special characteristic of seeking a low local minimum that for the local search methodology described above one may, for a large class of problems of practical and scientific importance, make the assumption that

$$\alpha^*=\text{maximum}_j\{\alpha_j\} \qquad (96)$$

Accordingly they made use of the following theorem to terminate the multi-start algorithm.

Theorem: Let *ir* be the number of sample (starting) points falling within the region of convergence of the current overall minimum F^{opt} after *it* points have been sampled. Then under the assumption given in (96) and a non-informative prior distribution, the probability that F^{opt} be equal to F^*, $Pr[F^{opt}=F^*]$, satisfies the following relationship:

$$Pr \geq q(it,ir)=1-(it+1)!(2\times it-ir)!/[(2\times it+1)!(it-ir)!] \qquad (97)$$

In practice a tolerance ε_F is prescribed in order to determine whether a newly obtained local minimum also corresponds to the current overall minimum F^{opt}. Thus, if at the end of the final inner trajectory, $|F^{k+1}-F^{opt}|<\varepsilon_F$, then the number of successes *ir* is stepped up by one. Also a prescribed target value q^* is set for $q(it,ir)$ so that once $q(it,ir)>q^*$ the global procedure terminates with $F^*:=F^{opt}$.

Once $\boldsymbol{x}^*(\mu)$, the global minimizer of the penalty function defined in (91) is found, it is a straightforward matter to determine the active constraints of the original constrained problem (90). The exact solution $\boldsymbol{x}^*$ to the constrained problem is then found by the one-time application of the trajectory method to the minimization of the sum of the squares of the residues of the active constraints, using $\boldsymbol{x}^*(\mu)$ as starting point.

9.3 The Particle Swarm Optimization algorithm

The second method used here for control purposes is a Particle Swarm Optimization (PSO) techniques, which belong to a relatively new class of evolutionary based search procedures that may be used to find the optimum solution $\boldsymbol{x}^*$ of the general optimization problem. The original PSO algorithm, proposed by Kennedy and Eberhardt in 1995, was inspired by the modelling of the social behaviour patterns of organisms that live and interact within large groups. In particular, PSO incorporates swarming behaviours

observed in flocks of birds, schools of fish, or swarms of bees. A PSO algorithm is easy to implement in most programming languages, since the core of the program can be written in a few lines of code. It has been proven to be both fast and effective, when applied to a diverse set of optimization problems. PSO algorithms are especially useful for parameter optimization in continuous, multi-dimensional search spaces.

In performing a search in the multi-dimensional space associated with the optimization problem of the form (89, 90), the PSO technique assigns direction vectors and velocities to each member (particle) of the swarm at their current positions. Each particle then "moves" or "flies" through the search space according to the particle's assigned velocity vector, which may be influenced by the directions and velocities of other particles in its neighbourhood. These localized interactions with neighbouring particles, propagate through the entire "swarm" of particles and results in the swarm as a whole moving to regions of the space closer to the solution of problem (89). The extent to which a particular particle influences other particles is determined by its so-called "fitness" along its trajectory of candidate solution points. The "fitness" is a measure assigned to each potential solution, and it indicates how good a particular candidate solution is relative to all other solution points. Hence, an evolutionary idea of "survival of the fittest" (in the sense of Darwinian evolution) comes into play, as well as a social behaviour component through a "follow the local leader" effect and emergent pattern formation (Farkas, Jármai 1997).

A more precise and detailed description of the particular PSO algorithm, as applied to penalty function formulation (91), and used in this study now follows.

Basic PSO Algorithm

1) Given M, k_{max}, $N_{max.}$ Set (time) instant k=0, $F_i^b = F^g = F_{before}^g = \infty$. Initialise a random population (swarm) of M particles (swarm members), by assigning an initial random position $\boldsymbol{x}_i^0$ (candidate solution), as well as a random initial velocity $\boldsymbol{v}_i^0$, to each particle i, i=1,2,…,M. Then compute simultaneous trajectories, one for each particle, by performing the following steps.

2) At instant k, compute the fitness of each individual particle i at discrete point $\boldsymbol{x}_i^k$, by evaluating $F(\boldsymbol{x}_i^k)$. With reference to the minimization (89), the lower the value of $F(\boldsymbol{x}_i^k)$, the greater the particle's fitness.

3) For i=1,2,…,M:
if $F(\boldsymbol{x}_i^k) \le F_i^b$ then set $F_i^b = F(\boldsymbol{x}_i^k)$ *and* $\boldsymbol{p}_i^b = \boldsymbol{x}_i^k$ {best point on trajectory i}
if $F(\boldsymbol{x}_i^k) \le F^g$ *then set* $F^g = F(\boldsymbol{x}_i^k)$ *and* $\boldsymbol{g}^b = \boldsymbol{x}_i^k$ {best global point}

4) If $F^g < F_{before}^g$ *then set* $N = 1$, *else set* $N = N + 1$.

5) If $N > N_{max}$ or $k > k_{\max}$ then STOP and set $\boldsymbol{x}^* = \boldsymbol{g}^b$; else continue.

6) Compute new velocities and positions for instant k+1, using the rule:
for i=1,2,…,M:

$$\boldsymbol{v}_i^{k+1} := \boldsymbol{v}_i^k + c_1 r_1 (\boldsymbol{p}_i^b - \boldsymbol{x}_i^k) + c_2 r_2 (\boldsymbol{g}^b - \boldsymbol{x}_i^k) \quad (98)$$

$$\boldsymbol{x}_i^{k+1} := \boldsymbol{x}_i^k + \boldsymbol{v}_i^{k+1} \quad (99)$$

where r_1 and r_2 are independently generated random numbers in the interval [0,1], and c_1, c_2 are parameters with appropriately chosen values.

7) Set $k = k + 1$ *and* $F_{before}^g = F^g$; go to step 2.

The technique is modified in order to be efficient in technical applications. It calculates discrete optima, uses dynamic inertia reduction and craziness for some particles [16].

10. Optimization results

Results obtained for continuous variables by the Snyman-Fatti global minimization algorithm are summarized in Table 1. The values of the parameters used are $\varepsilon_F=10^{-2}$, $q^*=0.99$ and $\mu=10^2$. For each case of n the box X was defined by: $750 \le x_1 \le 1250$; $750 \le x_2 \le 1250$; $7.5 \le x_3 \le 12.5$. The respective number of function-cum-gradient evaluations were 1860 for n=3, 1455 for n=4, and 1904 for n=5. The gradients were approximated using forward finite differences with variable perturbations of 10^{-3}.

Table 1 shows that the constraints ($g_j(\boldsymbol{x}) \le 0, \quad j = 1,..6$) are all effectively satisfied at the computed global minimum. However, different constraints are active for the different cases. For n=3 constraints 1, 2 and 6 are active, for n=4 constraints 1, 5 and 6 are active, and for n=5 the active constraints are 3, 4 and 5.

Table 1. Continuous results obtained by the global minimization algorithm. Dimensions and deflections in mm, stresses in MPa, costs in $

Results obtained for continuous variables by PSO are summarized in Table 2.

Table 2. Results obtained by PSO for continuous (cont) and discrete (disc) variables. Dimensions and deflections in mm, stresses in MPa, costs in $

The penalty parameter value was 1.0e8, the probability of craziness (% i.e: 0 - 100) was 1.5, the cognitive learning coefficient, (0.5-2) was 2.0, the social learning coefficient was 1.4, the dynamic inertia scale factor beta was 0.98. The function evaluations were required were about 20000-22000. Probability of craziness is similar, that of mutation at genetic algorithm. Its value is about 1-3 %.

Results obtained for discrete variables by PSO are summarized in Table 3.

The results clearly show that the optimal value for the number of internal stiffeners is n_{opt} = 4. The stress constraints are active for n = 3 and n = 5, the deflection constraint is active for n = 4. Activeness means not equality, but close value to the limit.
The continuous results are nearly identical and show the robustness of both techniques. At PSO some slight violations of the constraints may occur. Discrete results are also important for designers to apply them easily. Table 3 shows that the discrete results are close to the continuous ones. The distance depends on the number of available cross sections.

11. Conclusions

It has been assumed that a plate supported at four corners and stiffened by open section ribs can be modelled by a torsionless gridwork. In the case of square symmetry the equations of the force method can be significantly simplified. Halved rolled I-section stiffeners can be used with different dimensions for edge and internal ribs. The uniformly distributed normal load causes also local bending stresses in the base plate fields. For different prescribed values of design variables, that include base plate thickness as well as the dimensions of the edge and internal stiffeners, this model allowed for the evaluation of constraint violations relating to stresses in the base plate and in stiffeners as well as to deflections of stiffeners. Thus the total cost, which includes the material, the manufacturing and painting costs, could be minimized subject to these structural constraints using mathematical optimization techniques, in which fabrications constraints guaranteeing a suitable welding technology were also taken into account. In particular the cost function includes the material, welding and painting costs and is formulated as a function of the number of stiffeners in one direction (n). The costs are analyzed considering the fabrication sequence.

Since the derived formulae for constraint evaluation are different for different number of stiffeners, it was necessary to carry out the optimization separately for each stiffener number. Here the optimization was performed for number of stiffeners n = 3, 4 and 5 which allowed for the identification the minimum cost design with n = 4.

In giving nearly identical results, the two different mathematical function minimization methods used here, namely the Snyman-Fatti global optimization algorithm and the particle swarm optimization (PSO), prove to be suitably robust, reliable and sufficiently accurate methods for obtaining practical optimal designs for square stiffened plates .

Acknowledgements
The research work was supported by the Hungarian Scientific Research Foundation grants OTKA T38058 and T37941 and by the József Öveges scholarship OMFB 01385/2006, given by the National Office of Research and Technology (NKTH) and the Agency for Research Fund Management and Research Exploitation (KPI). The project was also supported by the Hungarian-South African Intergovernmental S&T co-operation program DAK 7/2002. The Hungarian partner is the Ministry of Education, R&D Deputy Undersecretary of State, and the South African partner is the National Research Foundation.

Appendix
Approximate formulae for UB profile dimensions

Calculation of b
y=a+blnx+c/lnx+d(lnx)^2+e/(lnx)^2+f(lnx)^3+g/(lnx)^3+h(lnx)^4+i/(lnx)^4
a= 4071797665.515043D0
b= -377581103.813262D0
c= -25351511152.9463D0
d= 17442666.41988002D0
e= 92925416774.55347D0
f= -155449.0539314809D0
g= -187087676930.7058D0
h= -10894.44641480538D0
i= 160167765716.8299D0

Calculation of t_f
y=a+bx+cx^2+dx^3+ex^4+fx^5+gx^6+hx^7+ix^8
a= -26.93815960004096D0
b= 0.7030053163805572D0
c= -0.0056933379440895 1D0
d= 2.383106250400329D-05
e= -5.605511588090933D-08
f= 7.662794270183799D-11
g= -5.902409057606285D-14
h= 2.267417890058806D-17
i= -2.999371273581411D-21

Calculation of t_w
y=a+bx+cx^2+dx^3+ex^4+fx^5+gx^6+hx^7+ix^8
a= 4.598131596507252D0
b= -0.1667245080692302D0
c= 0.00266225263859364 3D0
d= -1.662919423768273D-05
e= 5.42570607199179D-08
f= -1.003562930723944D-10
g= 1.063362616433473D-13
h= -6.028516559742138D-17
i= 1.419727612597333D-20

References

European Convention of Constructional Steelwork (ECCS) (1988) Recommendations for Steel Construction. Buckling of steel shells. No.56. Brussels.

Farkas J, Jármai K. (2003) Economic design of metal structures, Millpress, Rotterdam.

Farkas J, ,Jármai K. (1997) Analysis and optimum design of metal structures. Balkema, Rotterdam-Brookfield.

Farkas J, Jármai K, Snyman JA., Gondos Gy. Minimum cost design of ring-stiffened welded steel cylindrical shells subject to external pressure. In: Lamas A, Simoes da Silva L. editors. Proc. 3rd European Conf. Steel Structures, Coimbra, 2002, Universidade de Coimbra; 2002, 513-22.

Farkas J, Jármai K. (2005a) Optimum design of a welded stringer-stiffened cylindrical steel shell loaded by bending. In: Hoffmeister B, Hechler O, editors. Eurosteel 2005. Proc. 4th Eurospean Conference on Steel and Composite Structures. Maastricht, The Netherlands 2005. Aachen, Druck und Verlagshaus Mainz GmbH. Vol. A, 1.3-15 – 1.3-22.

Farkas J, Jármai K. (2005b) Optimum design of a welded stringer-stiffened steel cylindrical shell subject to axial compression and bending. Welding World; 49: (5-6), 85-9.

Farkas J. (2005) Economy of welded stiffened steel plates and cylindrical shells. J. Comput Applied Mechanics (Univ. of Miskolc); 6: (2) 183-205.

Groenwold AA, Snyman J.A. (2002) Global optimization using dynamic search trajectories. J Global Optimiz; 24:51-60.

Jármai K, Farkas J. (1999) Cost calculation and optimization of welded steel structures. J Constructional Steel Research; 50: 115-35.

Jármai K, Snyman JA., Farkas J. (2006) Minimum cost design of a welded orthogonally stiffened cylindrical shell. Computers Struct; 84: (12) 787-97.

Kennedy J & Eberhardt R. (1995) Particle swarm optimization. Proc. Int. Conf. on Neural Networks, Piscataway, NJ, USA, 1942-1948.

Schutte J.F., Groenwold A.A. (2005) A study of global optimization using Particle Swarms, Journal of Global Optimization; 31: 93–108

Snyman J.A. (1982) A new and dynamic method for unconstrained minimization. Applied Mathematical Modelling; 6; 449-462.

Snyman J.A. (1983) An improved version of the original leap-frog dynamic method for unconstrained minimization LFOP1(b). Applied Mathematical Modelling; 7; 216-218.

Snyman JA , Fatti L.P. (1987) A multi-start global minimization algorithm with dynamic search trajectories. J Optimiz Theory Appl; 54:121-41.

Snyman J.A., Kok S. (2007) A reassessment of the Snyman-Fatti dynamic search trajectory method for unconstrained global optimization, Submitted to Journal of Global Optimization.

Snyman J.A. (2005) Practical mathematical optimization, An introduction to basic optimization theory and classical and new gradient-based algorithms. *Springer Verlag*, New York, 257 p. ISBN 0-387-29824-x

Timoshenko S., Woinowsky-Krieger, S. (1959) Theory of plates and shells, New York-Toronto-London: McGraw Hill.

Figure captions

Figure 1. Schematic illustration of a stiffened square plate supported at four corners as well as the cross-sections of the edge and the internal stiffeners

Figure 2. Square plate with three internal stiffeners in one direction. Internal forces and deflections

Figure 3. Square plate with four internal stiffeners in one direction. Internal forces and deflections

Figure 4. Square plate with five internal stiffeners in one direction. Internal forces and deflections

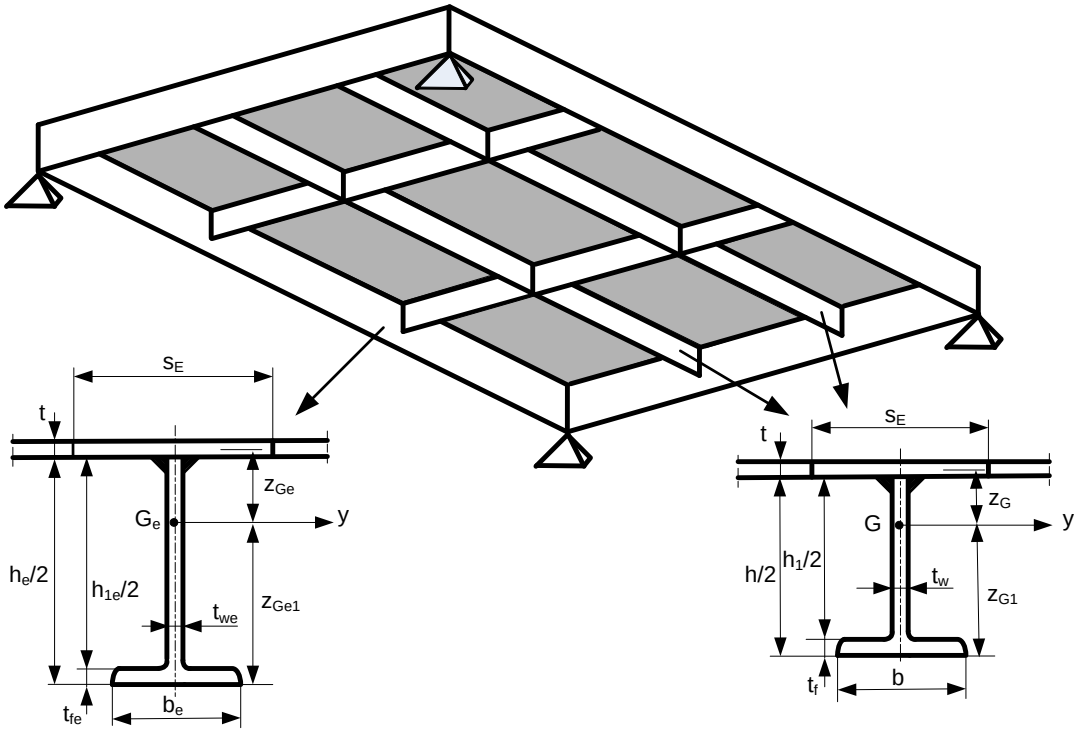

Figure 1. Schematic illustration of a stiffened square plate supported at four corners as well as the cross-sections of the edge and the internal stiffeners. The vertical plates symbolise the stiffeners.

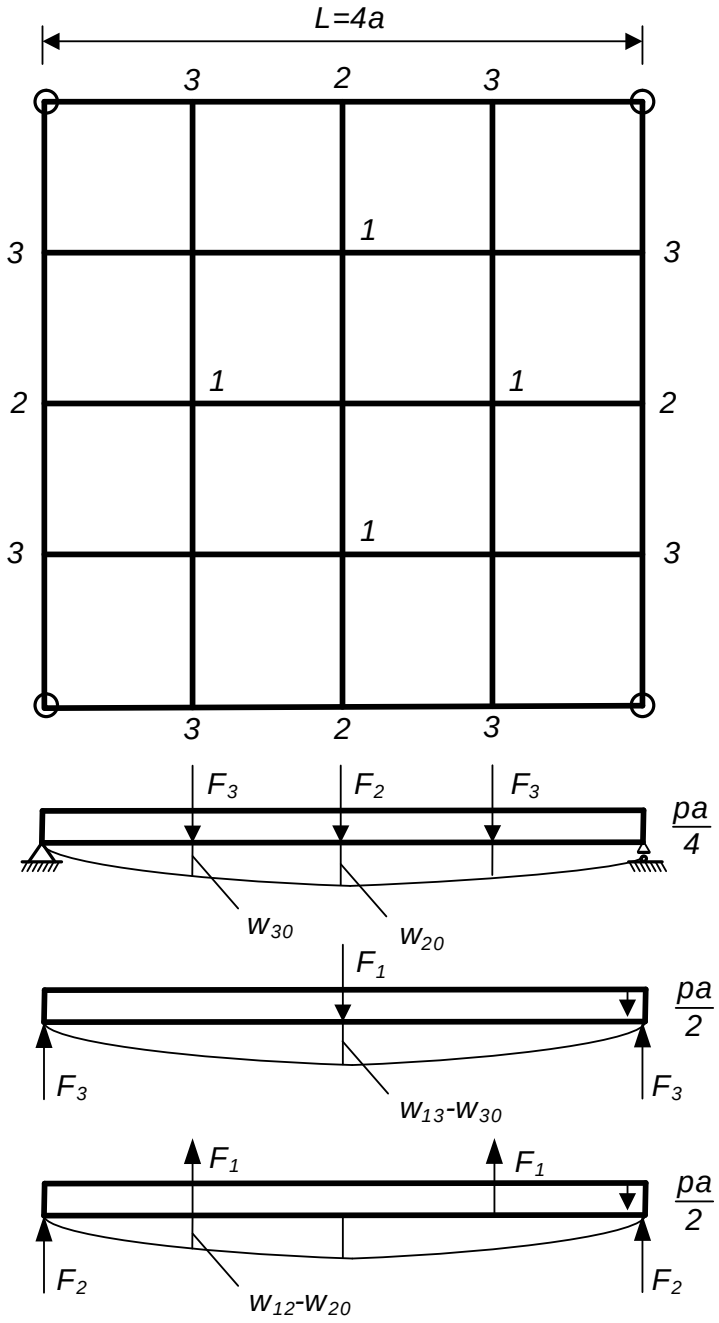

Figure 2. Square plate with three internal stiffeners in one direction. Internal forces and deflections

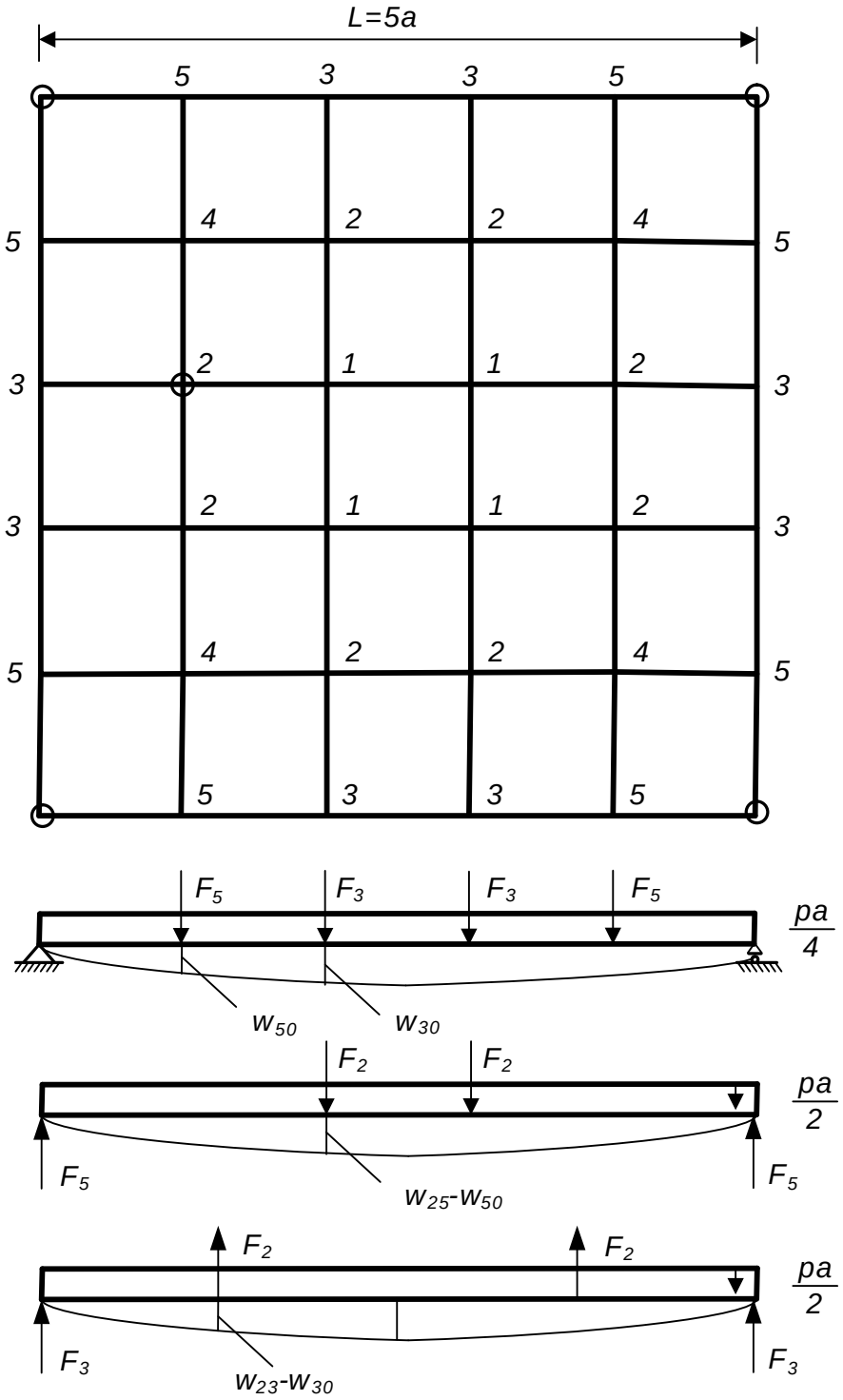

Figure 3. Square plate with four internal stiffeners in one direction. Internal forces and deflections

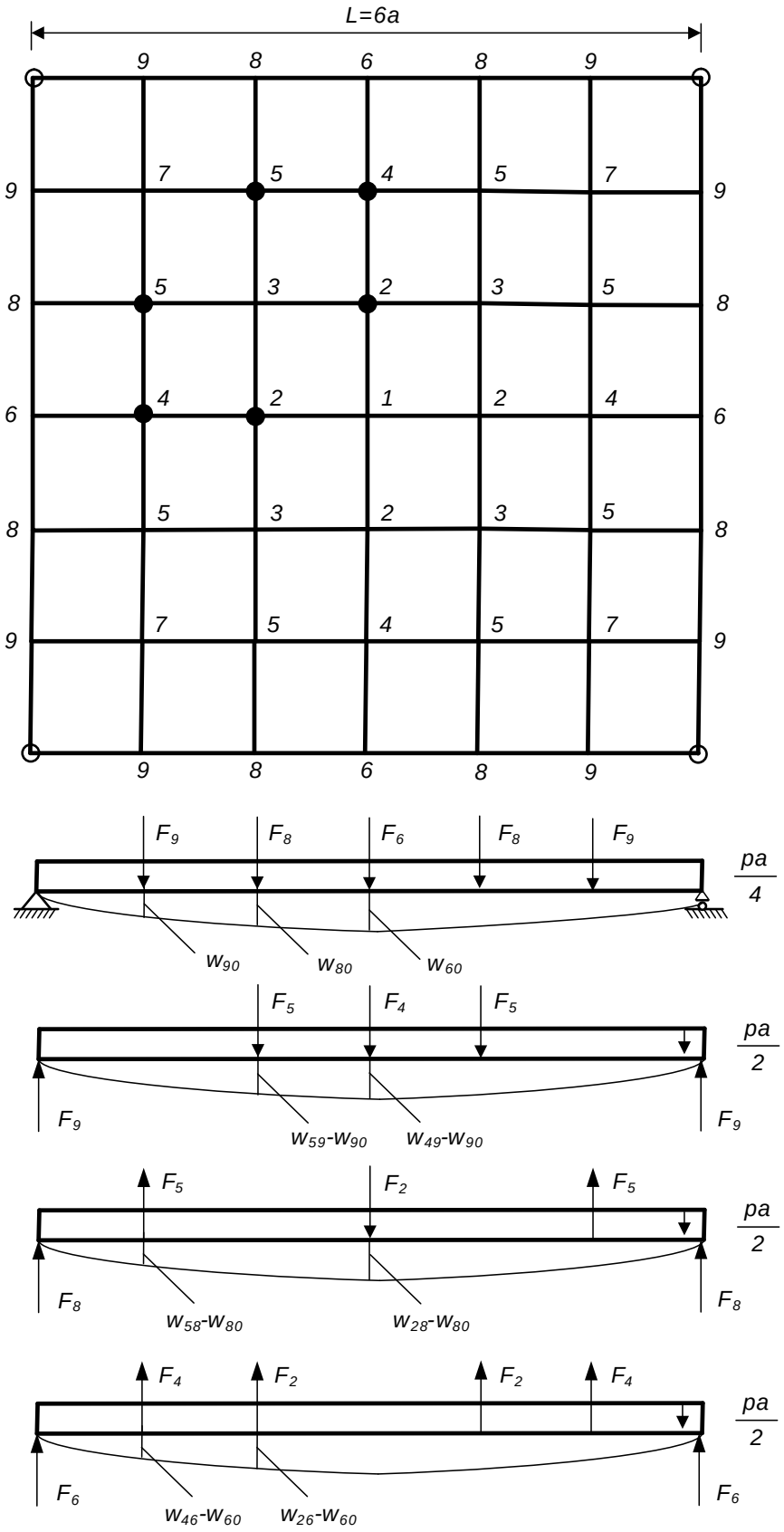

Figure 4. Square plate with five internal stiffeners in one direction. Internal forces and deflections

Table 1. Results obtained by the global minimization algorithm SF. Dimensions and deflections in mm, limit w_{meg} = 60 mm, stresses in MPa, limit f_{y1} = 322.72 MPa, costs in $

n	h_e	h	t	g_1	g_2	g_3	g_4	g_5	g_6	K
3	941.40	557.28	14.50	4.8E-4	5.5E-4	-223	-194	-7.8	2.5E-4	108423
4	1005.24	590.37	8.34	-6.2E-5	-206	-1.74	-112	2.4E-4	-9.5E-5	98271
5	961.47	778.46	11.98	-64	-128	9.0E-5	-1.2E-4	-7.6E-6	-95	122532

Table 2. Results obtained by PSO for continuous variables (cont). Dimensions and deflections in mm, limit w_{meg} = 60 mm, stresses in MPa, limit f_{y1} = 322.72 MPa, costs in $

n	h_e	h	t	σ_e	σ_{e1}	σ	σ_1	w_e	w_1	K
3 cont	941.75	557.33	14.49	321.72	322.23	99.12	128.61	52.16	59.99	108424.7
4 cont	1004.85	589.78	8.37	321.73	116.98	320.06	212.48	59.99	60.39	97994.6
5 cont	953.43	818.95	12.78	249.07	212.2	289.64	306.8	59.93	32.76	127210

Table 3. Results obtained by PSO with discrete (disc) variables. Dimensions and deflections in mm, limit w_{meg} = 60 mm, stresses in MPa, limit f_{y1} = 322.72 MPa, costs in $

n	h_e	h	t	σ_e	σ_{e1}	σ	σ_1	w_e	w_1	K
3 disc	980.	607.6	15	296.4	313.9	110.	148.	45.7	56.9	113489.9
4 disc	1008.1	607.6	9	296.1	222.2	280.9	201.0	56.1	50.5	101576.3
5 disc	1008.1	762.2	12	238.3	145.4	305.7	308.9	46.9	36.1	134165.5